Axisymmetric scalable magneto-gravitational trap for diamagnetic particle levitation[1]

J. P. Houlton,[1] M. L. Chen,[1] M. D. Brubaker,[2] K. A. Bertness,[2] C. T. Rogers[1]

[1]Department of Physics, University of Colorado Boulder, Boulder, Colorado 80309, USA

[2]National Institute of Standards and Technology, Boulder, Colorado 80305, USA

We report on the design, construction, and use of axisymmetric magnetic traps for levitating diamagnetic particles. The magnetic traps each consist of two pole pieces passively driven by a neodymium iron boron (NdFeB) permanent magnet. The magnetic field configuration between the pole pieces combined with the earth's gravitational field form a 3D confining potential capable of levitating a range of diamagnetic substances, e.g. graphite powder, silica microspheres, and gallium nitride (GaN) powder and nanowires. Particles trap stably at atmosphere and in high-vacuum for periods up to weeks with lifetimes largely determined by choices made to actively destabilize the trap. We describe the principles of operation, finite element design, approximate closed-form results for design rules, and examples of operation of such traps.

I. Introduction

Levitating and trapping of particles ranging from atoms to microscale objects has become a common technique for studying physical, chemical, and biological systems over the last century.[1–6] Recently, various trapping techniques have been used to levitate nano- and micro-mechanical systems to e.g. control mechanical motion and ultimately pursue studies of meso-scale quantum mechanical effects,[7–10] create highly sensitive detectors of force,[11] and assemble complex nano-structures.[12] Many trapping schemes e.g., optical tweezers, ion traps, and magneto-optical traps, involve active energy input and time varying configurations of electromagnetic fields and are often limited by the optical properties of materials to be trapped. However, it is possible to levitate and trap diamagnetic materials using only static configurations of magnetic fields[13] and without any restrictions on materials' optical properties. Since a very large number of substances exhibit diamagnetism,[14] diamagnetic trapping is a widely applicable solution for studying systems decoupled from their environments.

Stable magnetic traps for diamagnetic particles have been previously demonstrated in a variety of geometries.[10,13–21] Some of these traps utilize specialized magnetic materials and require complex machining to build. The time, materials, and skills required to design and fabricate such traps can be prohibitive and impede experimental progress. Other, simpler trap designs typically incorporate paramagnetic fluids in their sample chambers. These traps are certainly useful for studying systems which exist natively in aqueous solutions or are otherwise unaffected by them, but many systems (e.g. sensitive nano-mechanical systems) cannot be adequately characterized or used while submerged in a lossy fluid environment. There seems to be a clear need for a simple, flexible magnetic trap that can operate in air and in vacuum without the need for paramagnetic fluids. In this paper we describe a simple magnetic trap design capable of levitating a wide variety of diamagnetic substances. Our axisymmetric design uses commonly available materials and can be fabricated by a novice in only a few hours in a machine shop. It is designed to levitate objects in air, in high vacuum, and during the process of moving between atmospheric and vacuum conditions, making it well suited for studying sensitive systems isolated from lossy environments.

II. Trap Design

Magnetic forces on diamagnetic particles

To begin, we consider magnetic forces experienced by diamagnetic particles in magnetic fields. Working in SI units, a small diamagnetic particle of volume, V, and uniform, scalar volume magnetic susceptibility, χ, placed in an external magnetic field, $\vec{H} = \frac{\vec{B}}{\mu_0}$, develops an induced magnetic moment per unit volume, $\vec{M} = \chi\vec{H}$, opposed to the external magnetic field (note χ is negative for diamagnetic materials and usually small). The total magnetic dipole moment of the particle will then be $\vec{m} = \chi V\vec{H} = V\frac{\chi}{\mu_0}\vec{B}$. Recall that the force on a magnetic dipole in an external field, $\vec{B}$, is $\vec{F} = (\vec{m}\cdot\boldsymbol{\nabla})\vec{B}$, analogous to the force on an electric dipole in an electric field.[22] Using a vector calculus identity we can rewrite this as: $(\vec{m}\cdot\boldsymbol{\nabla})\vec{B} = \boldsymbol{\nabla}\left(\vec{m}\cdot\vec{B}\right) - \vec{m}\times\left(\boldsymbol{\nabla}\times\vec{B}\right) - \vec{B}\times(\boldsymbol{\nabla}\times\vec{m}) - \left(\vec{B}\cdot\boldsymbol{\nabla}\right)\vec{m}$. With static fields and no source terms and given $\vec{m} =$

$V\frac{\chi}{\mu_0}\vec{B}$, we know that $\boldsymbol{\nabla}\times\vec{B}=\boldsymbol{\nabla}\times\vec{m}=0$, and we now have $\vec{F}=V\frac{\chi}{\mu_0}(\vec{B}\cdot\boldsymbol{\nabla})\vec{B}=\boldsymbol{\nabla}\left(V\frac{\chi}{\mu_0}\vec{B}\cdot\vec{B}\right)-V\frac{\chi}{\mu_0}(\vec{B}\cdot\boldsymbol{\nabla})\vec{B}$ or $\vec{F}=\frac{1}{2}\boldsymbol{\nabla}\left(V\frac{\chi}{\mu_0}\vec{B}\cdot\vec{B}\right)$. The magnetic energy change, ΔU_M, of the dipole in moving from position $r_1=\infty$ to $r_2=R$ is: $\Delta U_M=-\int_{r_1}^{r_2}\vec{F}\cdot d\vec{r}=-\int_{\infty}^{R}\frac{1}{2}\boldsymbol{\nabla}\left(V\frac{\chi}{\mu_0}\vec{B}\cdot\vec{B}\right)\cdot d\vec{r}$. This integral can be evaluated to finally give the common expression for the energy of a diamagnetic particle in a static external B-field referenced to $U_M=0$ where $B=0$:[23]

$$U_M=-V\frac{\chi}{2\mu_0}B^2, \qquad (1)$$

where $B^2=\vec{B}\cdot\vec{B}$, and $B=\sqrt{B_x^2+B_y^2+B_z^2}$ is the magnitude of the magnetic field. The magnetic force felt by the particle, $\overrightarrow{F_M}=-\boldsymbol{\nabla}U_M$, will therefore be:

$$\overrightarrow{F_M}=V\frac{\chi}{2\mu_0}\boldsymbol{\nabla}B^2=V\frac{\chi}{\mu_0}(B\boldsymbol{\nabla}B). \quad (2)$$

Levitation conditions

For diamagnetic substances, where χ is negative, $\overrightarrow{F_M}$ will point in the direction of greatest decreasing field strength. If we wish to levitate a particle, the vertical component of $\overrightarrow{F_M}$ must balance the force of gravity, $\overrightarrow{F_g}=-mg\hat{z}$. That is we require that

$$F_{M,z}=V\frac{\chi}{\mu_0}(B\boldsymbol{\nabla}B)_z=mg, \quad (3)$$

where $(B\boldsymbol{\nabla}B)_z=B\frac{\partial B}{\partial z}$ and indicates the z component of $(B\boldsymbol{\nabla}B)$. Note, $(B\boldsymbol{\nabla}B)_z\neq B_z\frac{\partial B_z}{\partial z}$ in general. For a given diamagnetic material, the following condition on the magnetic field configuration is then needed to levitate it:

$$(B\boldsymbol{\nabla}B)_z=\frac{\rho g\mu_0}{\chi}, \quad (4)$$

where $\rho=m/V$ is the mass density of the material. For materials with anisotropic magnetic susceptibilities, χ is a tensor quantity, and a more complex treatment is needed. Table 1 shows the densities, magnetic susceptibilities and the $(B\boldsymbol{\nabla}B)_z$ values needed to achieve levitation for a few example substances.

Material	ρ (kg/m^3)	SI Volume Magnetic Susceptibility (10^{-6})	Levitation $(B\boldsymbol{\nabla}B)_z$ (T^2/m)
H_2O[24]	1,000	-9.05	1,360
SiO_2[25]	2,200	-11.28	2,400
GaN[26,27]	6,150	-20.4	3,710
Graphite[28]	2,270	-14	1,990
Mineral Oil[25]	878	-8.8	1,230

Table 1. Some example diamagnetic substances' mass densities, magnetic susceptibilities, and $(B\nabla B)_z$ values necessary to levitate against the earth's gravity. Note the value of χ for graphite here is smaller than the anomalously large value for pyrolytic graphite.

Levitation forces alone are not enough to trap particles. In order to achieve stable trapping in an axisymmetric geometry, we require a radial restoring force on particles displaced from the trapping center in addition to the vertical magnetic force. This leads to the following requirement:[23]

$$\frac{\partial^2 B^2}{\partial r^2} > 0, \quad (5)$$

i.e. we require a positive radial curvature of the magnetic field magnitude at the levitation point.

Example physical design and finite element model

Figure 1a shows a constructed magnetic trap which fulfills the radial stability condition of Equation 5 and produces $(B\nabla B)_z$ sufficiently large to levitate gallium nitride (GaN) particles. The trap itself consists of a 12.7 mm diameter 12.7 mm tall cylindrical neodymium iron boron (NdFeB) permanent magnet[29] and two pole pieces. The pole pieces are made of O-1 drill rod tool steel (with typical magnetic saturation levels of 1.0-1.5 T), which we model as iron with a magnetic saturation level of ~1.25 T[30], and were machined with typical dimensions as listed below.

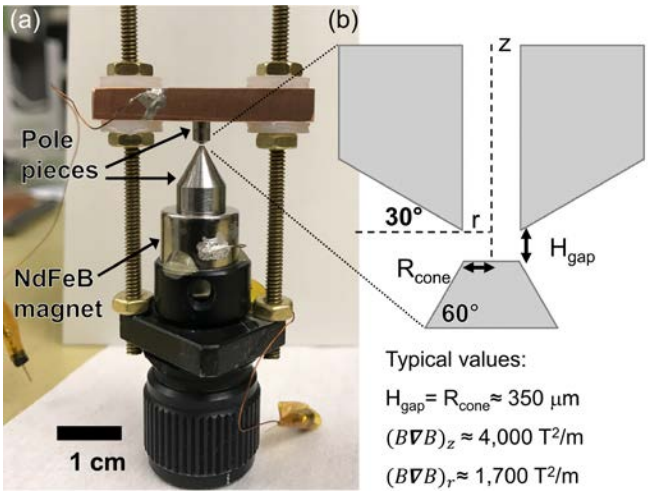

Figure 1. (a) Photograph of an assembled magnetic trap. The trap consists of a NdFeB permanent magnet and two pole pieces. The top pole piece is held in place by a copper support structure which is electrically isolated from the rest of the trap to allow electric field biasing across the two pole pieces to further control charged levitated particles. The magnet and bottom pole piece rest on a modified optical mount which allows the gap between the pole pieces to be adjusted. **(b)** Diagram of the trapping region between the pole pieces. The bottom pole piece is cone shaped to focus magnetic flux lines from the permanent magnet below. The flattened tip of the cone produces radial stability in the trapping forces. The top pole piece resembles a nozzle structure with a bore-hole down the center that matches the cone tip diameter and allows diamagnetic particles to drop down into the trapping region. Typical pole piece dimensions and magnetic fields are shown.

Figure 1b shows a close-in view diagram of the space between the pole pieces, where the magnetic trap forms. The cylindrical portion of the bottom pole piece (7.6 mm diameter and 3.6 mm height) captures magnetic flux lines from the magnet beneath it. The cone shaped portion of

the bottom pole piece (7.6 mm base diameter and 6.14 mm height) has a 60º taper that focuses the flux lines, enhancing the magnetic field strength. The bottom pole piece ends in a flattened tip with a designed radius, R_{cone}. The size scale of the cone tip determines the final magnetic field strength and levitation power, defined as $(B\boldsymbol{\nabla}B)_z$, of the trap (cf. [31]). The top pole piece sits a distance, H_{gap}, above the tip of the bottom pole piece and has a nozzle-like structure. The top pole piece has a bore-hole down the center with radius equal to R_{cone}, a 30º taper on the lower face, an outer diameter of 2.8 mm, and a total height of 5.0 mm. Typically, H_{gap} will be set to roughly R_{cone}. The top pole piece refocuses the magnetic field lines as they diverge out of the cone tip and increases the radial stability of the magnetic trap. Additionally, the bore-hole provides an easy delivery path for loading diamagnetic particles into the trapping region between the pole pieces. The top pole piece is suspended by a copper mounting structure and is electrically isolated from the rest of the magnetic trap. The permanent magnet and bottom pole piece rest on a modified optical mount which allows the spacing, H_{gap}, to be adjusted.

We used the Finite Element Method Magnetics (FEMM 4.2) software package[30] to calculate the magnetic field in our trap. We modeled the pole pieces using the pure iron material in the FEMM 4.2 materials library. The permanent magnet was modeled as grade N52 NdFeB with B_r =1.48 T Figure 2 shows simulation results of the space between the pole pieces in the physically realized magnetic trap from Figure 1a. In Figure 2a, the concave up, bowl shape of the field magnitude gives radial stability to the trap, and the large magnetic field (~2 T) and its rapid divergence give a $(B\boldsymbol{\nabla}B)_z$ in excess of 3,700 T^2/m, enough to levitate particles of GaN. This magnetic field configuration combined with the earth's gravitational field form a 3D confining potential energy per unit mass as seen in Figure 2b. This potential energy scales with the volume, V, of a particle in the trapping region. The trap's spring constant, k (restoring force per unit displacement from the trap center), will then be proportional to V. Since the mass, m, of a particle is also proportional to V, the trap frequency, $\frac{1}{2\pi}\sqrt{k/m}$, is approximately independent of particle size for small objects. The curvature of the energy surface in Figure 2b predicts radial trap frequencies for GaN particles of 25±2 Hz and a vertical trap frequency of 30±3 Hz.

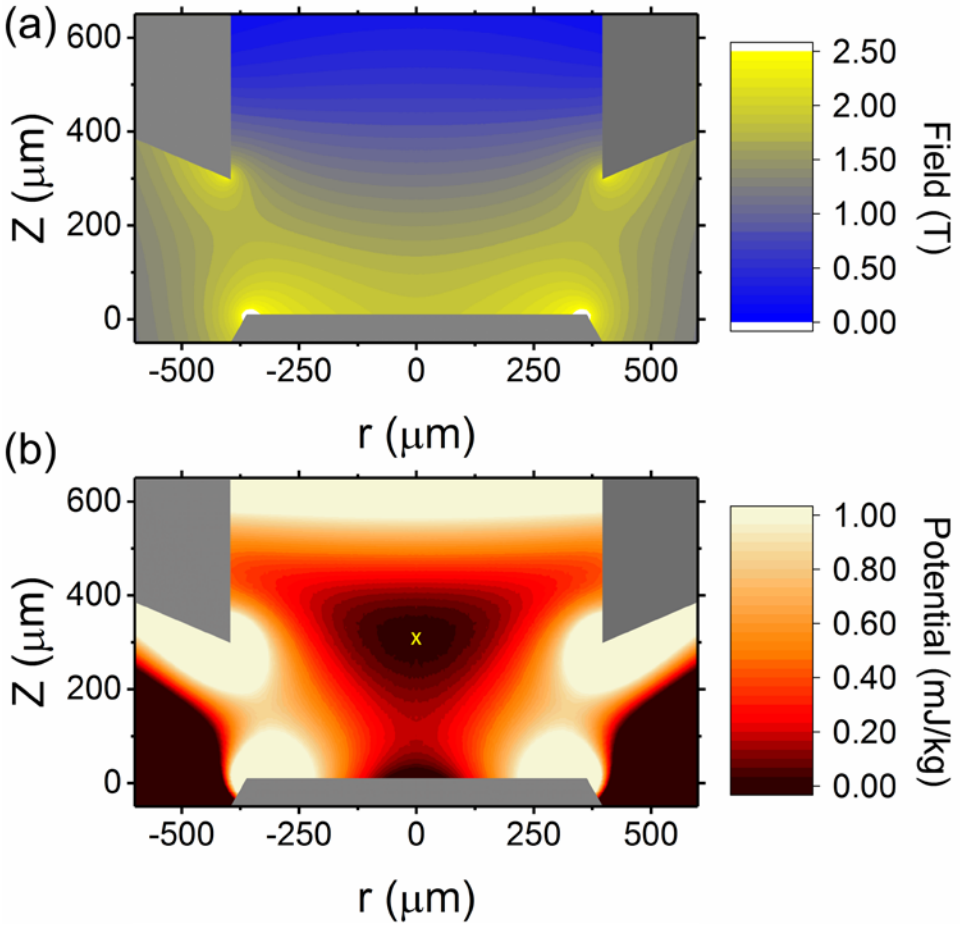

Figure 2. (a) Plot of the magnetic field strength between the pole pieces in a trap used to levitate GaN particles, shown as a two-sided axisymmetric slice. **(b)** Plot of the magneto-gravitational potential energy per unit mass for GaN inside the trap. The yellow "x" near the center of the plot indicates the trapping position of an electrically neutral GaN particle. The grayed out regions in (a,b) show the physical boundaries of the pole pieces.

Particle orientation

The orientation of trapped particles will depend on the natures of both the trapped material and the magnetic trap. In general, materials with anisotropic magnetic susceptibility will have preferred particle orientations in even a spherically symmetric magnetic trap. For non-spherically symmetric traps, non-spherical particles (even if they are magnetically isotropic) will have preferred orientations to minimize their energy in the trap. Some diamagnetic trap designs incorporate sample chambers filled with paramagnetic fluids to enhance trapping forces.[19–21,32–34] In such traps, buoyant forces on trapped particles introduced by the paramagnetic fluids depend on the density of the particles and can be used to measure densities of trapped materials and to produce density dependent orientations of trapped objects. Our trap operates in air at atmospheric pressure and under vacuum, without the need for paramagnetic buffer solutions, and will not show such density dependent effects on orientation. Our traps do exhibit ellipsoidal asymmetries (see Figure 2b) which will result in preferred levitation orientations for any non-spherical, diamagnetic particle.

Stability considerations

The trapping potential is deep enough for a wide range of particle sizes to be robust against a range of perturbing forces. A 10 μm diameter sphere of GaN, for example, placed in this potential will be trapped to a depth of roughly 10^{-15} J. Thermal fluctuations in the energy per mode of particle vibration will have a characteristic energy: $\frac{1}{2}k_B T$. For the approximately harmonically bound particle at 300 K, these fluctuations will be of order $4\text{x}10^{-21}$ J and will not be capable of knocking the example particle out of the trap. GaN particles down to 100 nm in diameter could be trapped before thermal fluctuations will be comparable to the trapping energy. Larger particles can be trapped as well until they are too big to fit within the physical dimensions of the trapping region. We have routinely trapped particles ranging in size from 1-100 μm.

Wind currents are an important concern for the stability of this magnetic trap when operating in air. The Stokes drag force, F_d, on a sphere of radius, R, in a fluid is given by:[35]

$$F_d = 6\pi\eta R v, \quad (6)$$

where η is the dynamic viscosity of the fluid and v is the flow velocity. For the example 10 μm particle trapped in air at atmospheric pressure and room temperature,[36] equation 6 suggests air currents at 1 cm/sec produce drag forces sufficient to overcome trap forces and blow the particle out of the trap. It is therefore important to keep the magnetic trap shielded from air currents. We typically operate ours in a closed box or vacuum chamber. When these magnetic traps are used in vacuum, care must be taken during the pump out process to throttle the pumping speed to ensure that trapped particles are not pulled from the trap by viscous drag.

The electric charge states of levitated particles are useful and also an important issue for trap stability.[16] A charged particle held in the magnetic trap will see image charge distributions in the metallic surfaces of the trap's pole pieces and will be attracted to them. For example, we estimate using Coulomb's law that a few micron sized particle with a net charge of ~1,000 elementary charges will feel an attractive force from its image charge in the cone pole piece sufficient to pull it from the magnetic trap center onto the cone tip. We apply static voltages of order 1-10 volts between the pole pieces to counteract this attractive force. An ionizing UV lamp in the holding chamber can produce ions to neutralize the levitated particle's charge. The application of voltages to the pole pieces is then no longer needed. Alternatively, a trapped particle can be allowed to keep its charge, and voltages between the pole pieces provide an active control on the particle's position in the trap.

Trapping different materials

Different diamagnetic substances require different $(B\boldsymbol{\nabla}B)_z$ in order to levitate as shown by Equation 4 and Table 1. Our magnetic trap design can be used to trap many different kinds of diamagnetic materials. For substances which require larger levitating power (i.e. larger $(B\boldsymbol{\nabla}B)_z$) to float, a smaller R_{cone} is needed. We simulated various sized traps to understand the levitation power as a function of size scale. Figure 3a shows the simulation results of varying R_{cone} on the maximum $(B\boldsymbol{\nabla}B)_z$ achieved in the trap. In this series of simulations we held $H_{gap} = R_{cone}$, used the same permanent magnet and cone taper angle, and kept the bore radius of the top pole piece

equal to R_{cone}. The magnetic field in the trapping region diverges over a length scale proportional to the cone tip radius, and so $(\boldsymbol{\nabla} B)_z \propto 1/R_{cone}$. For large values of R_{cone}, the B-field at the cone tip surface is determined by the reduction in cross-sectional area from the bottom of the cone to the top, and B $\propto 1/R_{cone}^2$. Thus for larger values of $R_{cone,}$ the levitation power scales as $1/R_{cone}^3$, as indicated by the dashed, blue trend line in Figure 3a. As R_{cone} becomes smaller, magnetic saturation effects in the pole pieces limit the growth of the B-field at the cone tip surface to roughly a constant. So, for smaller values of R_{cone}, the levitation power of the trap scales as $1/R_{cone}$, as indicated by the red, dot-dashed trend line in Figure 3a. Traps with cone tip radii between 100 μm and 1 mm are easy to fabricate and can levitate a host of common diamagnetic materials. Given a diamagnetic material to be levitated, one simply chooses the appropriate R_{cone} size.

Once a trap is constructed, its levitation power can be tuned by adjusting the spacing between the pole pieces, H_{gap}, and keeping all other trap parameters the same. Figure 3b shows the effect of tuning H_{gap} for a trap with a 400 μm radius cone tip. The resulting levitation power can be tuned by roughly a factor of 2. This tunability is useful when the magnetic susceptibility of the material to be levitated is not known precisely, when one wishes to levitate multiple different substances using a single trap, and to compensate for machining tolerances during trap construction.

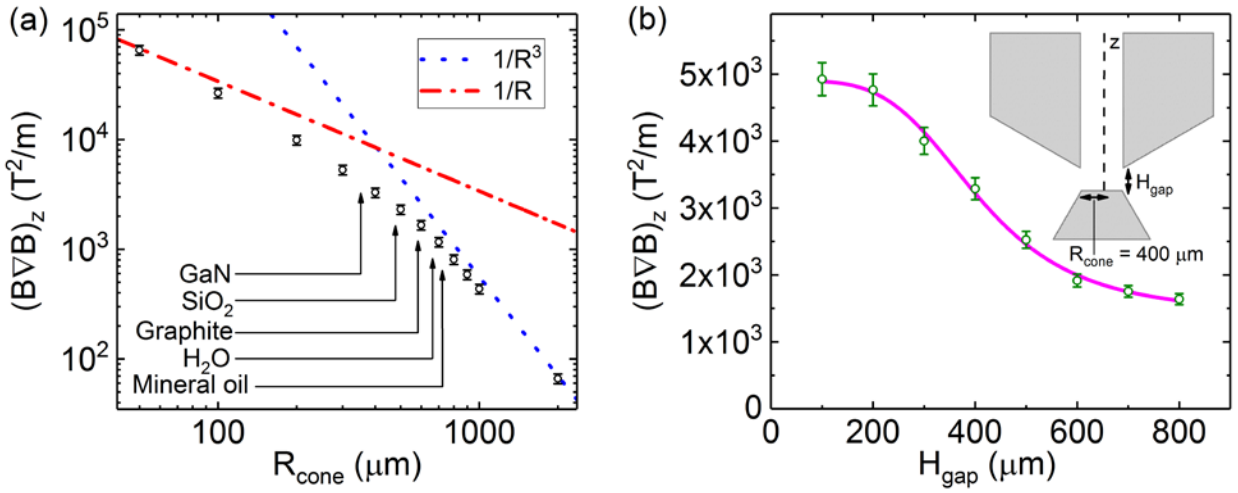

Figure 3. (a) Simulation results (black, open circles) showing the maximum values of $(B\boldsymbol{\nabla} B)_z$ (i.e. the maximum levitation power of the trap) for variable R_{cone} while holding $H_{gap} = R_{cone}$, using the same permanent magnet and cone taper angle, and keeping the bore radius of the top pole piece equal to R_{cone}. The fields necessary to levitate a few example materials are indicated. The 1/R and 1/R^3 trend lines show the approximate scaling of maximum $(B\boldsymbol{\nabla} B)_z$ with R_{cone} for smaller and larger cone tip sizes respectively. **(b)** Simulation data (green, open circles) showing the effect of varying $H_{gap}$for a fixed R_{cone} on the maximum value of $(B\boldsymbol{\nabla} B)_z$. By changing the spacing between a given set of pole pieces, one can tune the levitation power of the trap across roughly a factor of 2. The solid magenta line shows a fit to the data of the form: $\frac{A}{1+(H_{gap}/R_{cone})^n} + const$ with $A = 3{,}500 \pm 200\ T^2/m$, $R_{cone} = 407 \pm 10\ \mu m$, $n = 4.1 \pm 0.6$, and $const = 1{,}400 \pm 100\ T^2/m$.

III. Trap Operation and Experimental Results

Loading the trap

We load particles into the magnetic trap by dropping them down the center bore-hole of the top pole piece. Although more sophisticated techniques can be used to load particles into traps such as ultrasonic horns,[10,16,37] piezoelectric dispensers,[18] and laser desorption,[9] we have had great success by simply dusting particles into the top pole piece using a cotton swab loaded with the desired material. Particles a few microns in size quickly reach terminal velocities in air (cf. Equation 6) on the order of 0.5 mm/s as they fall through the center bore of the pole piece. Roughly 10 seconds later, particles make their way through the pole piece into the trapping region and come to a halt. When loading a magnetic trap by this technique, it is important to exercise patience. Particles with high charge states often tend to fall out of the trapping region and onto the cone tip due to their electrostatic attraction to the metallic cone surface and the image charge therein. Since initially neutral microparticles can be quite rare, it is useful to apply a bias voltage across the pole pieces during the initial stage of trapping and then neutralize the levitated particle's charge before removing the bias voltage. Particles then levitate indefinitely in the trap's static magnetic field. We have stably trapped a variety of particles at atmospheric pressure and in high vacuum for days at a time.

Observing levitated particles

Our trap design allows optical access to the trapping region from the side and the top for easy imaging of particles. Figure 4 shows optical micrographs of a variety of levitated diamagnetic particles in these magnetic traps. Motion within the traps, whether purposely driven or Brownian in nature, is apparent for small particles (see below). In Figure 4a, a levitated ~200 μm clump of graphite powder can be seen under white light illumination. In Figures 4b-d, red laser light is used to illuminate the smaller, trapped particles. We have found that a combination of white light and red laser illumination is helpful for imaging trapped particles across a wide size range (~1-100 μm). The levitated single GaN nanowire seen in Figures 4c, 4d in side view and top view respectively is observed to float with its *c*-axis (the long axis of the nanowire) preferentially vertically oriented. This behavior was consistent for the many single GaN nanowires that we levitated. Given the trapping potential's ellipsoidal shape, a magnetically isotropic nanowire would float with its long axis horizontally oriented in order to minimize its energy. The observed vertical orientation indicates that it is energetically favorable for the nanowire to be misaligned with the trapping potential's shape and to instead align the *c*-axis of the nanowire with the local magnetic field direction, i.e. vertical. This is an indication that the *c*-axis of wurtzite GaN has a weaker diamagnetic susceptibility than the *a*-axis.

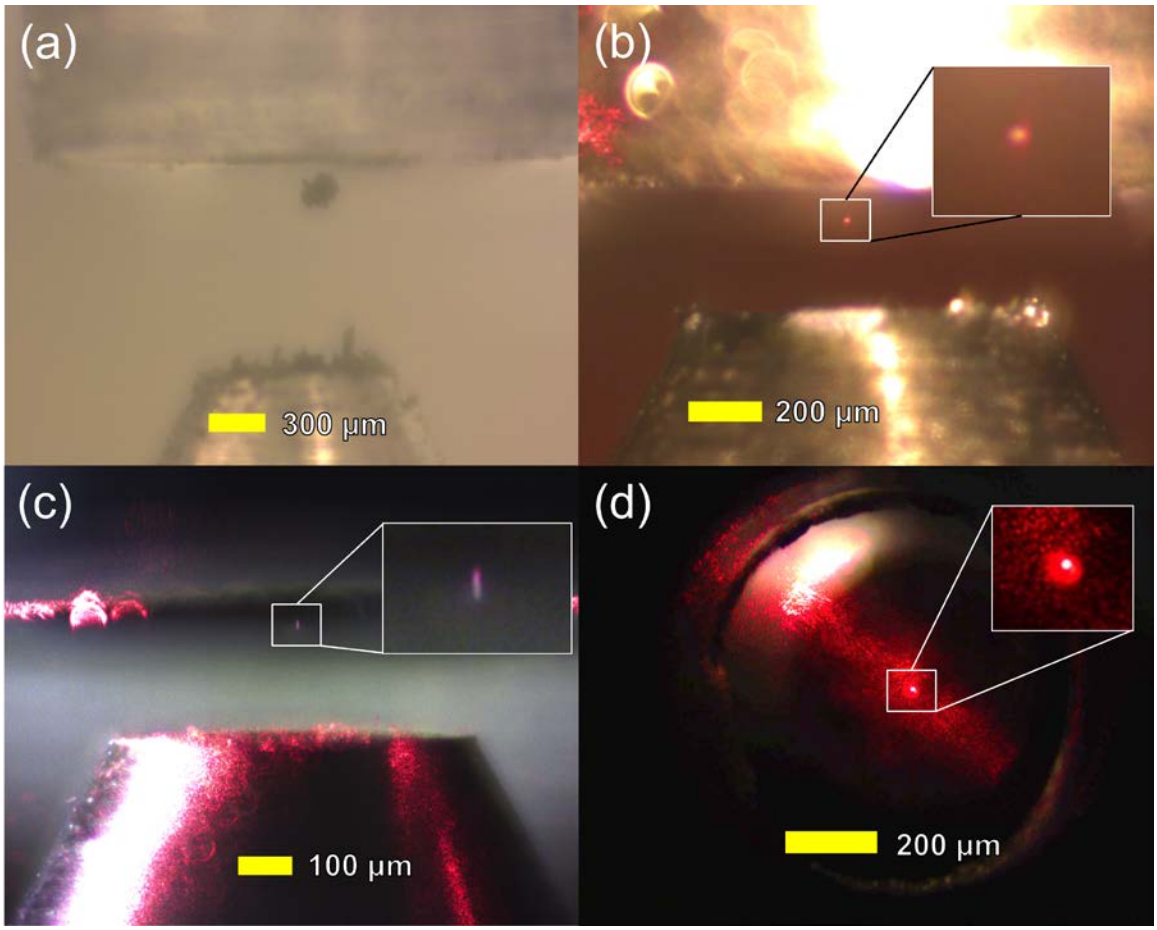

Figure 4. Optical micrographs of various diamagnetic particles levitating between the pole pieces of magnetic traps. The insets are each ~2.5X zoom. **(a)** Side view of a levitated clump of graphite powder illuminated with white light. The scale bar is 300 µm. **(b)** Side view of a levitated 3 µm radius silica microsphere illuminated with white light and red laser light. The scale bar is 200 µm. **(c)** Side view of a single floating *c*-axis GaN nanowire illuminated with white light and dim red laser light. The *c*-axis of the nanowire is preferentially vertically oriented, indicating the *c*-axis of GaN has a weaker diamagnetic susceptibility than the *a*-axis. The scale bar is 100 µm. **(d)** Top view through the bore of the trap's top pole piece showing a single GaN nanowire illuminated by red laser light. The scale bar is 200 µm.

Studying motion in the trap

Once particles are successfully loaded into the magnetic trap, they can be studied as desired. For example, we have used these traps to study Brownian motion, to study vibration modes of isolated objects, and as a simple pre-trapping method to prepare particles for subsequent laser trapping. Figure 5 is an example of center of mass motion studies of GaN flakes levitated at atmospheric pressure and under modest vacuum conditions in the trap. Figure 5 shows a plot of the power spectral density (PSD) of the center of mass motion of a GaN flake inside the magnetic trap at atmospheric pressure. The motion of the particle was captured by digital video recording and was analyzed using tracking software to produce time records of its position. Fourier analysis of these time records gives a PSD consistent with an overdamped Brownian driven particle of mass $3x10^{-14}$ kg at a temperature of 300 K in a harmonic oscillator potential. Figure 6a (Multimedia view) shows a still frame of the video footage used in this analysis. Upon pumping the holding chamber down to a pressure of 0.4 Pa, the trapped particle's motion is no longer overdamped. We measure the motion of the particle by imaging it onto a position

sensitive photodiode. The particle is observed to undergo noisy radial oscillations at a characteristic frequency of 26.2 ± 0.2 Hz, as seen in the inset PSD in Figure 5. Using simulation data, we estimate the radial trap frequency for GaN particles in this trap to be 25± 2 Hz. This is consistent with the experimental results. Figure 6b (Multimedia view) shows a still frame of top view video footage of the GaN particle undergoing noisy trap oscillations.

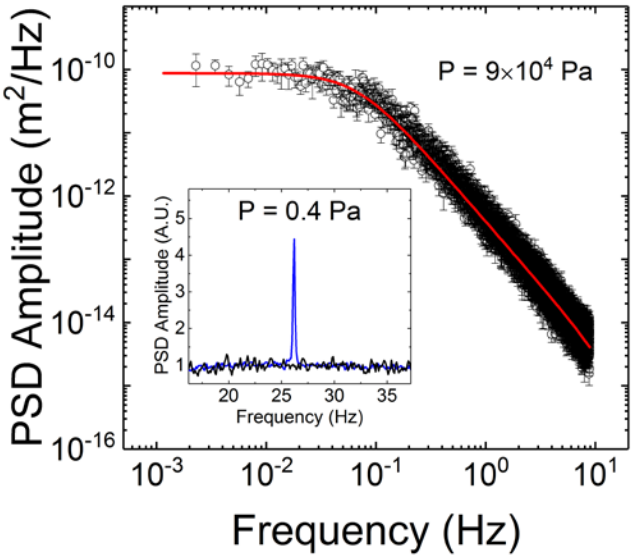

Figure 5. Power spectral density (PSD) plot of the radial motion of a GaN particle trapped in air at atmospheric pressure. The black circles are data derived from radial position tracks taken from a video of the particle's motion in the trap. The solid red curve is an overdamped Lorentzian fit to the data, consistent with heavily damped Brownian motion of a particle of mass $3x10^{-14}$ kg in a harmonic oscillator potential. The inset figure shows a PSD plot of the GaN particle's radial motion after pumping the holding chamber down to a pressure of 0.4 Pa (the blue line). The black line shows the background signal when no particle is present in the trap. The particle is observed to undergo underdamped, periodic, orbital motion within the trap at a characteristic frequency of 26.2 ± 0.2 Hz, consistent with the simulation-estimated radial trap frequency of 25 ± 2 Hz.

When particles are trapped in a vacuum environment their motion in the trap will be less damped. Small perturbations to a particle can build up and produce significant center of mass motion. For example, a small amount of visible laser light incident on a levitated graphite particle will produce radiometer forces,[38] i.e. differential heating of the particle's front and back sides upon illumination which results in differences in gas impact momentum transfer and significant forces at partial vacuum pressures. We have observed radiometer forces on graphite particles held at 3 Pa pressures capable of sending them into large orbits within the trap. Figures 6c and 6d (Multimedia view) show a ~50 μm graphite particle at rest and in orbital oscillation respectively when roughly 0.1 W/cm^2 of 640 nm laser light is focused on it. The particle orbits in the trap rather than simply being displaced from the trapping center due to a combination of effects. First, a small tilt of the magnetic trap away from the vertical leads the graphite particle to float slightly off center in the magnetic trap. Second, the propagation direction of the illumination laser is misaligned with respect to the radial direction of the trap. When the laser is turned on, radiometer forces cause the particle to jet forward with a non-radial initial velocity. The particle then moves in an orbital path around the trap, losing energy constantly due to drag forces but getting a large kick of energy every time it passes back through the focal point of the laser.

It is clearly important to exercise caution when particles are levitated in vacuum to ensure that they are not accidentally driven into oscillations that would knock them out of the magnetic trap. Mechanical vibrations of the magnetic trap by vacuum pumps and optical forces from lasers used for illumination are two common sources of particle excitation that should be carefully controlled in order to maintain reliable trapping.

Multiple particles can be levitated simultaneously and studied in this trap design if desired. Particles will either clump together in the trap center or remain separated and spread out depending on their electric charge states. Figure 6e (Multimedia view) shows three silica microspheres levitating in a rough vacuum of 40 Pa. The microspheres are similarly charged and repel each other, forming a spread out but stable configuration in the magnetic trap. Interactions and self-assembly within multi-particle systems e.g. Coulomb crystal formation[39] could be readily studied in these magnetic traps.

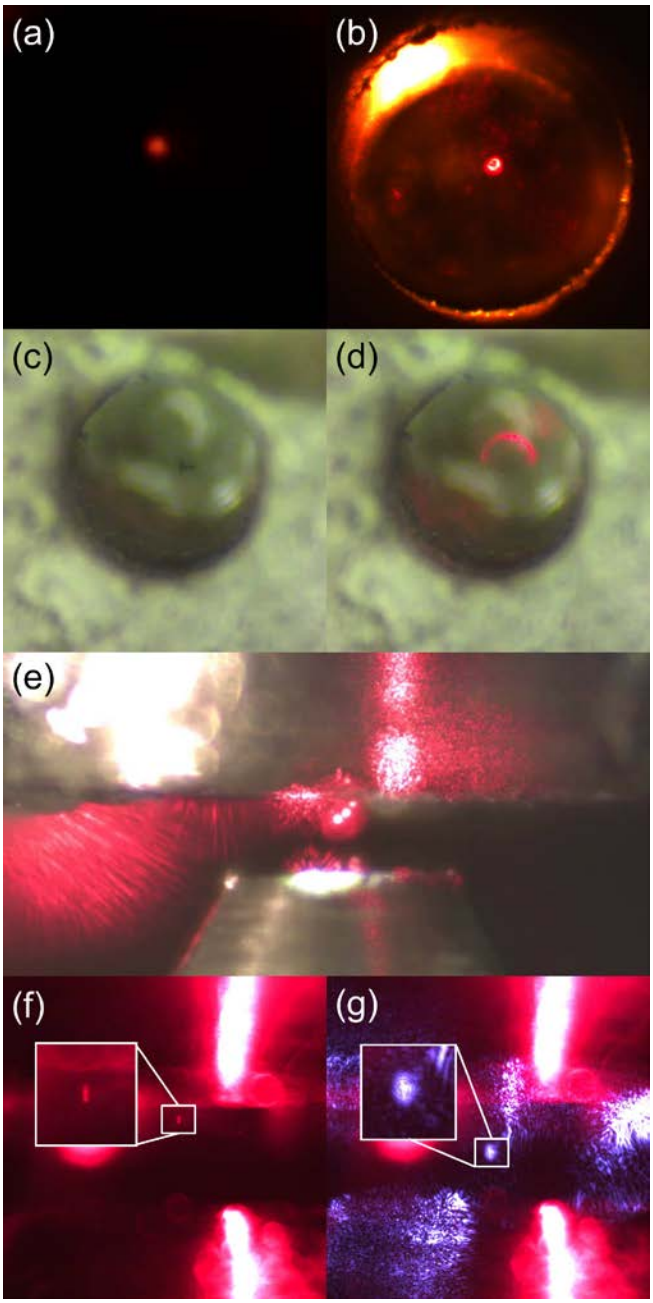

Figure 6. (a) Side view of a roughly 3μm GaN particle trapped at atmosphere undergoing Brownian motion (Multimedia view). **(b)** Top view of GaN particle held at 0.4 Pa as it is driven into noisy trap oscillations (Multimedia view). **(c)** Top view of a levitated graphite flake held at 3 Pa roughing vacuum pressure. **(d)** Graphite flake in radial orbital motion in trap. Illumination with laser light produces radiometer forces capable of sending the flake into large orbits within the trap (Multimedia view). **(e)** Multiple silica microspheres with similar charge states held at 40 Pa roughing vacuum pressure. The like-charged spheres repel each other and spread out in the trap but are all trapped stably (Multimedia view). **(f)** Side view of GaN NW levitating at atmospheric pressure at its equilibrium position of the magnetic trap. **(g)** The same NW upon turning on an optical trap and dragging the NW downward. When the optical trap is removed, the NW returns to its original position in **(f)** (Multimedia view).

The trap design also allows the input of optical trap beams from the side with numerical apertures (NA) typically as high as ~0.44, allowing the magnetic trap to be used as a preliminary loading and selection stage for later, stiffer optical trapping. An example of this functionality can be seen is Figure 6. Figure 6f shows a GaN NW levitating at atmospheric pressure at the equilibrium positon of the magnetic trap. Figure 6g (Multimedia view) shows the same NW upon turning on an optical trapping beam. The optical trap used here is approximately 10 mW of 852 nm laser light focused to a 1 μm beam waist (NA of 0.27) and exerts greater trapping forces on the NW than the magnetic trap. When the optical trap is translated down, the NW is dragged with it, away from its magnetic equilibrium position. When the optical trapping beam is turned off, the NW rises back up to its original position in the magnetic trap. Using the magnetic trap in conjunction with optical tweezers allows additional control over levitated particles. The magnetic trap provides a convenient loading mechanism for the optical tweezers and allows one to investigate and select particles before optical trapping. Additionally, the magnetic trap provides a long-term, passive storage mechanism when the optical trap is removed, maintaining a sample's isolation from its environment and preserving it for future measurement.

IV. Conclusion

In summary, we have designed and demonstrated a simple magnetic trap for levitating diamagnetic particles. These traps are appropriate for experiments on a wide variety of physical systems, and most any diamagnetic material can be trapped using this design by choosing the correct trap size scale. Our trap design is made with commonly available materials, is simple to fabricate, and operates without the use of paramagnetic fluids. We have constructed multiple magnetic traps and demonstrated their ability to levitate several different target substances including graphite, silica, and GaN. The demonstrated ability to levitate different materials along with analysis of trapped particle motion confirms the validity of magnetics simulations used to design these traps. Particles can be held indefinitely at atmosphere and in vacuum. This trap design allows easy incorporation of imaging and optical experiments, e.g. optical tweezers, making it an excellent first trapping stage for later, stiffer optical trapping. These traps show promising capability and can be applied to study many systems in isolation from their environments.

We gratefully acknowledge support for these studies by the National Institute of Standards and Technology (NIST) under award number 70NANB15H352 and by a Research & Innovation Seed Grant from the University of Colorado Boulder.

References

[1] R.A. Millikan, Phys. Rev. **2**, 109 (1913).

[2] H.S. W. Paul, Zeitschrift Für Naturforsch. A **8**, 448 (1953).

[3] A. Ashkin, J.M. Dziedzic, J.E. Bjorkholm, and S. Chu, Opt. Lett. **11**, 288 (1986).

[4] A. Ashkin, J.M. Dziedzic, and T. Yamane, Nature **330**, 769 (1987).

[5] M.H. Anderson, J.R. Ensher, M.R. Matthews, C.E. Wieman, and E.A. Cornell, Science (80-.). **269**, 198 (1995).

[6] B.C. Sawyer, B.L. Lev, E.R. Hudson, B.K. Stuhl, M. Lara, J.L. Bohn, and J. Ye, Phys. Rev. Lett. **98**, 1 (2007).

[7] D.E. Chang, C.A. Regal, S.B. Papp, D.J. Wilson, J. Ye, O. Painter, H.J. Kimble, and P. Zoller, Proc. Natl. Acad. Sci. U. S. A. **107**, 1005 (2009).

[8] G. Planes Conangla, A.W. Schell, R.A. Rica, and R. Quidant, Nano Lett. (2018).

[9] S. Kuhn, A. Kosloff, B.A. Stickler, F. Patolsky, K. Hornberger, M. Arndt, and J. Millen, Optica **4**, 356 (2017).

[10] B.R. Slezak, C.W. Lewandowski, J.-F. Hsu, and B. D'Urso, New J. Phys. **20**, (2018).

[11] G. Ranjit, D.P. Atherton, J.H. Stutz, M. Cunningham, and A.A. Geraci, Phys. Rev. A **91**, (2015).

[12] P.J. Pauzauskie, A. Radenovic, E. Trepagnier, H. Shroff, P. Yang, and J. Liphardt, Nat. Mater. **5**, 97 (2006).

[13] A.K. Geim, M.D. Simon, M.I. Boamfa, and L.O. Heflinger, Nature **400**, 323 (1999).

[14] M.D. Simon, L.O. Heflinger, and A.K. Geim, Am. J. Phys. **69**, 702 (2001).

[15] P. Kauffmann, P. Pham, A. Masse, M. Kustov, T. Honegger, D. Peyrade, V. Haguet, and G. Reyne, IEEE Trans. Magn. **46**, 3293 (2010).

[16] J.F. Hsu, P. Ji, C.W. Lewandowski, and B. D'Urso, Sci. Rep. **6**, 1 (2016).

[17] O. Gunawan, Y. Virgus, and K.F. Tai, Appl. Phys. Lett. **106**, (2015).

[18] H. Chetouani, H. Rostaing, G. Reyne, C. Jeandey, V. Haguet, and C. Dieppedale, IEEE Trans. Magn. **42**, 3557 (2006).

[19] C. Zhang, P. Zhao, F. Gu, J. Xie, N. Xia, Y. He, and J. Fu, Anal. Chem. **90**, 9226 (2018).

[20] A. Winkleman, K.L. Gudiksen, D. Ryan, G.M. Whitesides, D. Greenfield, and M. Prentiss, Appl. Phys. Lett. **85**, 2411 (2004).

[21] A.B. Subramaniam, D. Yang, H.-D. Yu, A. Nemiroski, S. Tricard, A.K. Ellerbee, S. Soh, and G.M. Whitesides, Proc. Natl. Acad. Sci. **111**, 12980 (2014).

[22] D.J. Griffiths, *Introduction to Electrodynamics*, 3rd ed. (Prentice Hall, 2005).

[23] M.D. Simon and A.K. Geim, J. Appl. Phys. **87**, 6200 (2000).

[24] G.P. Arrighini, M. Maestro, and R. Moccia, J. Chem. Phys. **49**, 882 (1968).

[25] M.C. Wapler, J. Leupold, I. Dragonu, D. Von Elverfeld, M. Zaitsev, and U. Wallrabe, J. Magn. Reson. **242**, 233 (2014).

[26] S.Y. Davydov, Semiconductors **36**, 41 (2002).

[27] T. Sahu, S.K. Nayak, and R.N. Acharya, Phys. B **173**, 257 (1991).

[28] N. Ganguli and K.S. Krishnan, Proc. R. Soc. **177**, 168 (1940).

[29] K.& J. Magnetics, N52 NdFeB axially magnetized, https://www.kjmagnetics.com/proddetail.asp?prod=D88-N52.

[30] D. C. Meeker, Finite Element Method Magnetics, Version 4.2 (11Apr2012 Build), http://www.femm.info.

[31] C. Pigot, H. Chetouani, G. Poulin, and G. Reyne, IEEE Trans. Magn. **44**, 4521 (2008).

[32] K. a Mirica, S.S. Shevkoplyas, S.T. Phillips, M. Gupta, and G.M. Whitesides, 10049 (2009).

[33] J.V.I. Timonen, A.F. Demirörs, and B.A. Grzybowski, Adv. Mater. **28**, 3453 (2016).

[34] J.V.I. Timonen, C. Raimondo, D. Pilans, P.P. Pillai, and B.A. Grzybowski, Nanoscale Horizons **2**, 50 (2017).

[35] H. Goldstein, C. Poole, and J. Safko, *Classical Mechanics* (2007).

[36] R.B. Montgomery, J. Meteorol. **4**, 193 (1947).

[37] R.R. Perron, IEEE Trans. Sonics Ultrason. **14**, 149 (1967).

[38] J.R. Brock, J. Colloid Interface Sci. **25**, 564 (1967).

[39] H. Thomas, G.E. Morfill, V. Demmel, J. Goree, B. Feuerbacher, and D. Möhlmann, Phys. Rev. Lett. **73**, 652 (1994).